Construction and Building Materials 319 (2022) 126092

Contents lists available at ScienceDirect

Construction and Building Materials

journal homepage: www.elsevier.com/locate/conbuildmat

CLT concrete composite floors with steel kerf plate connectors

Md Shahnewaz [a,*], Robert Jackson [a], Thomas Tannert [b]

[a] Fast+Epp, Vancouver, Canada
[b] School of Engineering, University of Northern British Columbia, Prince George, Canada

ARTICLE INFO

Keywords:
Timber concrete composite
Cross-laminated timber
Shear capacity
Connections

ABSTRACT

This paper presents experimental investigations on timber-concrete-composite (TCC) floors with transversely installed steel kerf plates as shear connectors. The TCC system was comprised of 245 mm thick, 7-ply cross-laminated timber (CLT) panels with 150 mm concrete topping. Three embedment depths of the steel kerf plates in CLT (35 mm, 70 mm, and 90 mm) were evaluated at hand of 18 small-scale shear tests. It was shown to be beneficial to only engage the top layer of the CLT panel in order to avoid rolling shear failure. Subsequently, two full-scale TCC floor segments were tested under symmetric four-point bending. The tests confirmed that the TCC floors with steel kerf plates can be designed using the established gamma procedure, and that they exhibited adequate capacity and stiffness to provide an economical solution. The results from this research were utilized to make project-specific design decisions for "The Arbour", a 10-storey mass timber building for George Brown College, located in Toronto, Canada.

1. Introduction

1.1. Objective

The potential of using engineered wood products for larger and non-residential structures with longer floor spans is increasingly being explored in Canada [1,2]. The resulting challenges, e.g. the increased demand on floor serviceability, can be addressed by the use of innovative materials such as cross-laminated timber (CLT) [3,4] and composite systems such as timber-concrete composite (TCC) floors [5,6]. The availability of CLT offers designers greater versatility in terms of architectural expression and structural performance. One challenge with CLT is the very low shear strength in the radial direction perpendicular to the grain, known as rolling shear, which can cause cracks in locations of high shear stresses such as column supports [7,8]. The Canadian standard for engineering design in wood CSA-O86 [9] provides specified rolling shear strength values for CLT varying from 0.43 to 0.63 MPa based on stress grade. A method to increase the panel shear capacity at high shear stress locations and prevent shear failure is to add reinforcing self-tapping screws (STS) which exhibit high axial stiffness [10,11]. Numerous solutions from low to high stiffness' are available as composite connectors, such as STS, dowel-type shear keys, perforated steel plates, or transverse notches. One of the main challenges with TCC floor systems is their cost when using shear connectors that are time-consuming to install.

The main objective of the research program presented herein was to investigate TCC floors systems with steel kerf plates as shear connector. The specific goals were to determine the appropriate embedment depth of the steel kerf plates into CLT panels, and to demonstrate that the strength and stiffness of the TCC floors can be adequately predicted using the gamma method in conjunction with the shear connector's stiffness parameters.

1.2. Background

George Brown College commissioned an educational building, "The Arbour", located in Toronto, Canada, to host classrooms, lecture halls, and the Tall Wood Institute [12]. The building will be one of the first tall timber buildings (52.5 m high above grade) to proceed with "assembly occupancy" in Canada. To reflect the building's purpose, timber was chosen as the primary structural material with CLT-concrete composite panels as the primary floor system. To eliminate the use of beams, 7-ply CLT panels span 9.2 m in north–south direction (Fig. 1), and act compositely with 150 mm structural concrete as a TCC 'slab band'. These floors will be supported on wide glulam columns (or "wallumns"), sized to reduce the weak-axis bending in the panels. Thinner 7-ply CLT panels run perpendicular to these bands with 50 mm non-structural concrete topping.

* Corresponding author at: Fast + Epp, 300 - 397 W 7th Avenue, Vancouver, BC V5Y 1M2, Canada.
E-mail addresses: md.shahnewaz@alumni.ubc.ca (M. Shahnewaz), rjackson@fastepp.com (R. Jackson), thomas.tannert@unbc.ca (T. Tannert).

https://doi.org/10.1016/j.conbuildmat.2021.126092
Received 14 May 2021; Received in revised form 6 December 2021; Accepted 9 December 2021
Available online 18 December 2021

1.3. Timber concrete composite floor systems

Deflection and vibration often govern the design of wooden floor systems. Previous studies have shown that TCC floors can overcome some of the inefficiencies associated with traditional reinforced concrete or light wood frame floors regarding strength, section depth, stiffness, and vibration performance [13]. TCC systems are generally comprised of timber elements (beam or panel) connected to a concrete layer by means of a shear connector.

TCC systems can be designed using EN 1995 [14], based on the γ-method [15]. This composite action can be quantified by the parameter γ, ranging from 0 (no composite action) to 1 (full composite action), cf. Equation (1). This parameter, together with cross-sectional properties of timber and concrete, allow estimating the TCC floor system's effective bending stiffness $(EI)_{\text{eff}}$, cf. Equation (2).

$$\gamma = \frac{1}{1 + \frac{\pi^2 E_c A_c s}{kL^2}} \tag{1}$$

$$(EI)_{eff} = E_c I_c + \gamma E_c A_c a_c^2 + E_t I_t + \gamma E_t A_t a_t^2 \tag{2}$$

where, E_c, E_t, I_c, I_t and A_c, A_t are the moduli of elasticity, second moment of inertia, and cross-section area for concrete and timber components, L is the floor span, k is the slip modulus of the connector, s is the connector spacing, and a_c and a_t are the distances from the neutral axis of the composite section to the neutral axis of the concrete and timber layers, respectively.

A wide range of TCC systems have been extensively studied in recent years, using mechanical connectors such as bolts [16,17], lag screws [18] or self-tapping screws (STS) either vertically installed and primarily acting in shear, or inclined and primarily acting in withdrawal [19,20], glued-in perforated steel plates in the context pf the proprietary HBV system [21], composite connectors [22], adhesive bonds [23], or hybrid screw/bonded systems [24]. An innovative connection with different combinations of steel plates with vulcanized rubber layers, which was used to be glued onto the timber beam surface, was deemed suitable for structural application [25] and its long-term behaviour was subsequently investigated [26]. The adopted shear connection can provide dry-type connection which can be assembled using screws on-site.

The basic phenomena governing the mechanical behavior of TCC connections with dowel type fasteners are similar, however, some relevant specificities have a non-negligible influence on the structural performance [18]. One challenge associated with the use of mechanical fasteners is cost and constructability [27]; therefore, recent research has focused on notched connections, e.g. [28,29]. Among different connection systems, notched connections were claimed to be both structurally superior and cost effective [29].

Compared with traditional timber floors, TCC floors using timber panels have improved strength, stiffness, durability, sound, and fire performance [28]. While initial work has focused on laminated-veneer lumber as engineered wood products used in TCC floor systems, Siddika et al. [30] summarize the state of the art of TCC floor systems involving CLT and conclude that such floors exhibit good performance under various loading conditions if adequately designed and constructed. Jiang et al. [28] demonstrated that a theoretical calculation method based on the gamma-method is suitable for CLT-concrete composite floors.

Traditional dowel-type fasteners, commonly used in connection systems but are relatively flexible, whereas notches cut into the wood and direct gluing are relatively rigid. Practitioners, however, are still reluctant to implement structural solutions that are governed by brittle wood strength or adhesive durability; therefore research on innovative mechanical connections is still ongoing, e.g. [28,29].

One alternative shear connection solution for TCC floors are steel kerf plates. High load-carrying capacity and high stiffness has been reported for these connectors in the only available publication dating back to 2001 [31]. Given their economics, practitioners have recently "rediscovered" this solution, and the Microsoft Silicon Valley Campus was the first building in North America where steel kerf plates were applied as shear connectors for TCC floor systems [32]. However, there is no published information available on the performance of steel kerf plates in CLT panels, and the effect of embedment depth into the CLT. The present study aims to fill this research gap.

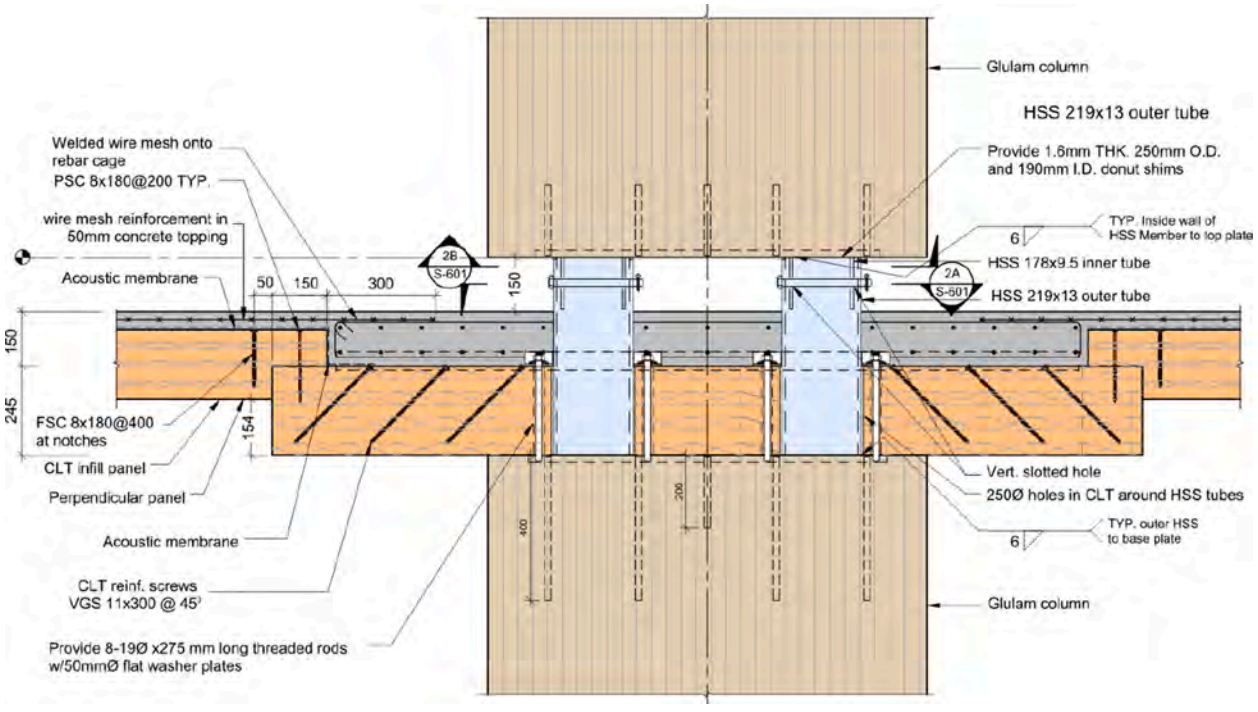

Fig. 1. Composite slab and glulam connection.

2. Experimental investigations

2.1. Materials

The TCC floors were comprised of 7-ply, 245 mm thick CLT panels. The CLT was grade E1M5 according to the Canadian standard for engineering design in wood CSA-O86 [9], manufactured according to PRG320 [33] with SPF (Spruce-Pine-Fir) lumber, 2100 Fb-1.8E machine-stress rated grade for the major strength axis laminations and SPF No.3 grade stock for the minor strength axis laminations. The relevant material properties (E-modulus, specified tension, compression, bending and shear strengths) were in the major strength axis $E = 12400$ MPa, $f_t = 17.7$ MPa, $f_c = 19.9$ MPa, $f_b = 30.5$ MPa, $f_v = 0.5$ MPa and in the minor strength axis $E = 9500$ MPa, $f_t = 5.5$ MPa, $f_c = 11.5$ MPa, $f_b = 11.8$ MPa, $f_v = 0.5$ MPa according to CSA-O86 [9]. The floors were supported on 430 × 1178 mm Douglas Fir glulam columns, grade 16c-E [9].

The TCC composite was completed with 150 mm concrete topping with 35 MPa minimum specified strength. Type I Portland cement was used with a maximum aggregate size of 10 mm and superplasticizer to achieve a high-flow, 80 mm slump. Concrete cylinder compression tests were conducted according to ASTM C39 [34] on day 7 after pouring (2 tests), day 28 (3 tests) and day 34 (the day of testing, 3 tests); the average strengths and coefficients of variation (CoV) were recorded as 33 MPa (CoV = 2.8%), 47 MPa (CoV = 2.7%) and 50 MPa (CoV = 1.5%), respectively. The concrete layer for both small- and full-scale specimens was reinforced with 10 M longitudinal rebar at top and bottom spaced 150 mm on centre, and 10 M transverse rebar (stirrups) spaced 300 mm on centre.

The steel kerf plates used as TCC connectors were grade A36 [35], 6 mm thick, and with a length and depths corresponding to the respective test specimens. These steel plates were installed into 7 mm wide kerf at 5° back bevel without the use of any adhesive.

One structural challenge with CLT is the very low shear strength in the radial direction perpendicular to the grain, known as rolling shear, which can cause premature rolling shear failure in locations of high shear stresses [7,8]. The rolling shear strength for E1M5 CLT specified in CSA-O86 [9] is only 0.5 MPa. One method to increase CLT panel shear capacity is to add reinforcing STS [10,11]. Herein, to prevent rolling shear failure, the full-scale CLT panels were reinforced with STS 11 × 300 mm [36] installed at an angle of 45^0.

2.2. Test series overview

A comprehensive test program as shown in Table 1 was designed to investigate the steel kerf plates as shear connectors for the implementation of a low-cost and efficient TCC system in the Arbour. The CLT specimens were prepared by Structurlam, in Penticton, while the concrete was poured by Datoff Bros Construction Ltd, Prince George. The tests were conducted at the University of Northern British Columbia Wood Innovation and Research Laboratory in Prince George.

Table 1
Test Series.

Series	Description	Test Type	#of tests	L [mm]	b_c [mm]	b_t [mm]
S1-A	Small-scale with 35 mm connector depth	Shear	6	1000	300	300
S1-B	Small-scale with 70 mm connector depth	Shear	6	1000	300	300
S1-C	Small-scale with 90 mm connector depth	Shear	6	1000	300	300
S6	Full-scale	Bending	2	9630	2200	2400

2.3. Small scale tests

Small-scale tests were conducted to investigate the shear capacity, stiffness and failure mechanism of TCC with steel plates. Steel kerf plates, 6 mm thick and 200 mm long, were installed in the CLT in 35 mm deep and 7 mm wide saw kerf at 5^0 back bevel as shown in Fig. 2. Three varying embedment depths into - a) full first layer of CLT (35 mm), b) full second layer of CLT (70 mm), and c) partial third layer of CLT (90 mm).

The test set-up consisted of a compression load frame, shown in Fig. 3. Test specimens were rotated by 12° similar to the procedure suggested in EN-408 [37], so that the resultant forces of loading and support are aligned. The loads were applied according to a modified EN-26891 [38] protocol at a displacement controlled rate of 5 mm/min. Specimens were loaded to approx. 40% (120 kN) of the estimated capacity, then unloaded to approx. 10% (30 kN) of estimated capacity, and finally loaded to failure, defined as the point when load dropped to 80% of the maximum. The actuator load and the relative vertical displacements between CLT and concrete were measured using two calibrated LVDTs (one in the front and one in the back), attached at mid-height of the specimens. The reported displacements are the averages between the front and the back measurements. The connector performance was analyzed at the maximum load F_{max}, displacement at maximum load d_{Fmax}, and two stiffness values serviceability (elastic) stiffness K_{ser} computed for the range between 10% and 40% of F_{max}, ultimate stiffness K_u computed for the range between 0% and 60% of F_{max}. In addition, the yield load F_y and the displacement at yield d_y were determined based on equivalent energy elastic plastic (EEEP) curves [39]. The ductility μ was calculated as the ratio of ultimate (d_u) to yield (d_y) displacement from the EEEP curves.

2.4. Full scale tests

The full-scale TCC floor systems consisted of CLT panels reinforced using 11 × 300 mm screws at 300 mm on centre, fully embedded into CLT for the outer 1/3rd of the spans. The TCC floors were 2100 mm long and 75 mm deep steel kerf plates are placed at 300 mm for the outer one-third spans and 1000 mm for the middle span, cf. Fig. 4. The 6 mm thick steel plates were ASTM A36 grade [35] installed into 35 mm deep and 7 mm wide kerf at 5^0 back bevel where the plates were fully embedded into the outer layer of CLT without the use of any adhesive.

The two specimens were tested under four-point bending. The schematic test setup is illustrated schematically in Fig. 5. The floors were connected to 430 × 1178 mm glulam columns by 12–16 mm Ø, 250 mm long glued-in threaded rods. The glulam columns in turn were connected to the concrete strong floor by angle brackets with anchor bolts. Loads were applied to the floors at approximately one-third points using four actuators with a maximum combined capacity of 1500 kN. The actuator loads are distributed equally using steel beams and a timber spreader as shown in Fig. 5b. A displacement-controlled load with a constant rate of 15 mm/min was applied. Specimens were loaded to approx. 40% of the estimated capacity, then unloaded to approx. 10% of estimated capacity, and finally loaded to failure, where failure was defined as the point when load dropped to 80% of the maximum.

A total of 20 sensors were attached to record the vertical deflection of the floor specimens and relative slip at the concrete to CLT interface, cf. Fig. 5a. LVDTs L1 to L4 measured the interface slips at the four corners and L5-L8 measured slips at the one-third loading points. String pots recorded the vertical deflections: 2 at mid-span (sensors D2/D5), 4 at one-third points (sensors D1/D6; D3/D4), 3 on the right side of the slab end (sensors D7-D9) to record the weak axis warping of the panels, and 3 string pots were installed on the left side of the slab end (sensors D10-D12) to record the weak axis warping of the panels.

The load increase from 10 to 40% of maximum force (F_{max}), $\Delta F_{10\text{-}40}$, and the corresponding increase in deflection, $\Delta d_{F10\text{-}40}$, allowed calculating the apparent bending stiffness EI_{app} using Eq. (3):

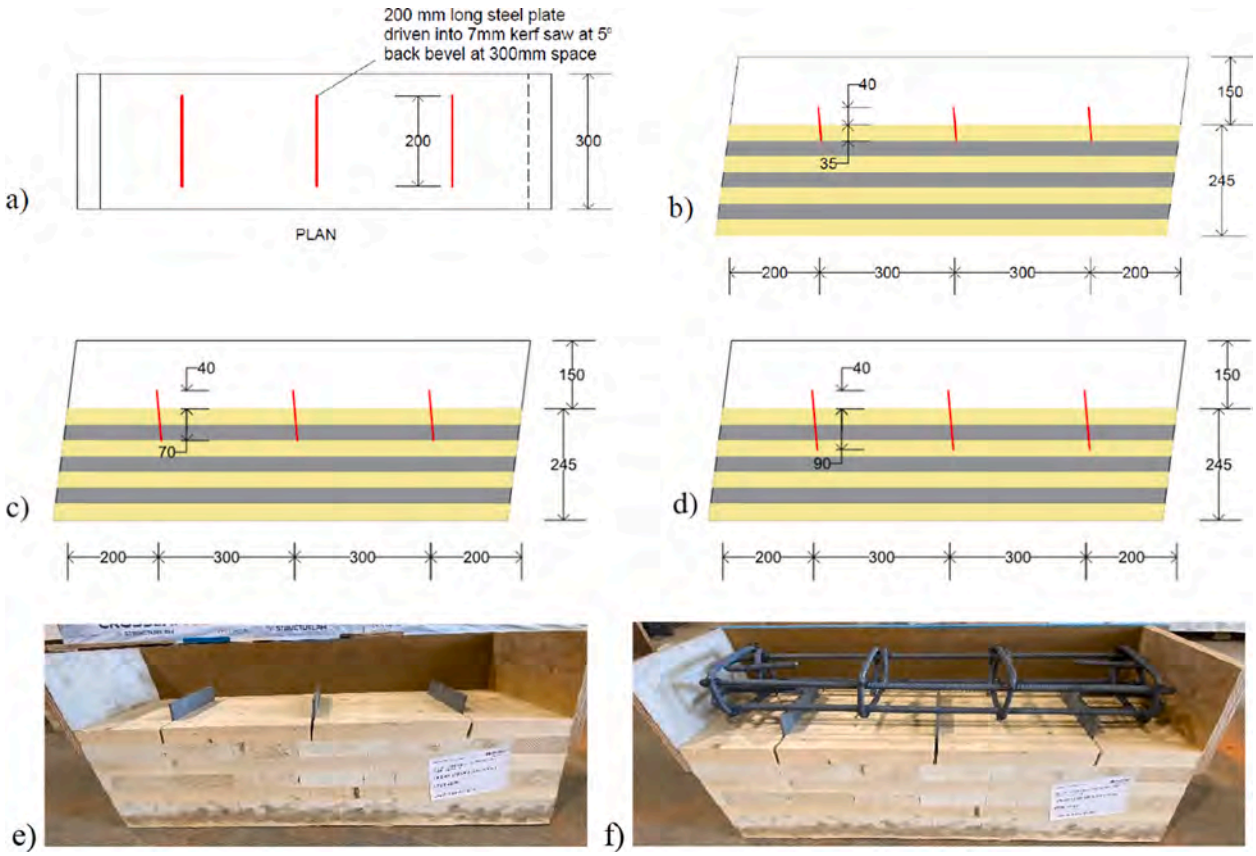

Fig. 2. Small-scale tests: (a) plan view with steel plates, (b) S1-A with 35 mm steel embedment into CLT, (c) S1-B with 70 mm steel embedment into CLT, (d) S1-C with 90 mm steel embedment into CLT; photo of a CLT panel with: (e) steel plates, and (f) steel plates and rebar before concrete pouring.

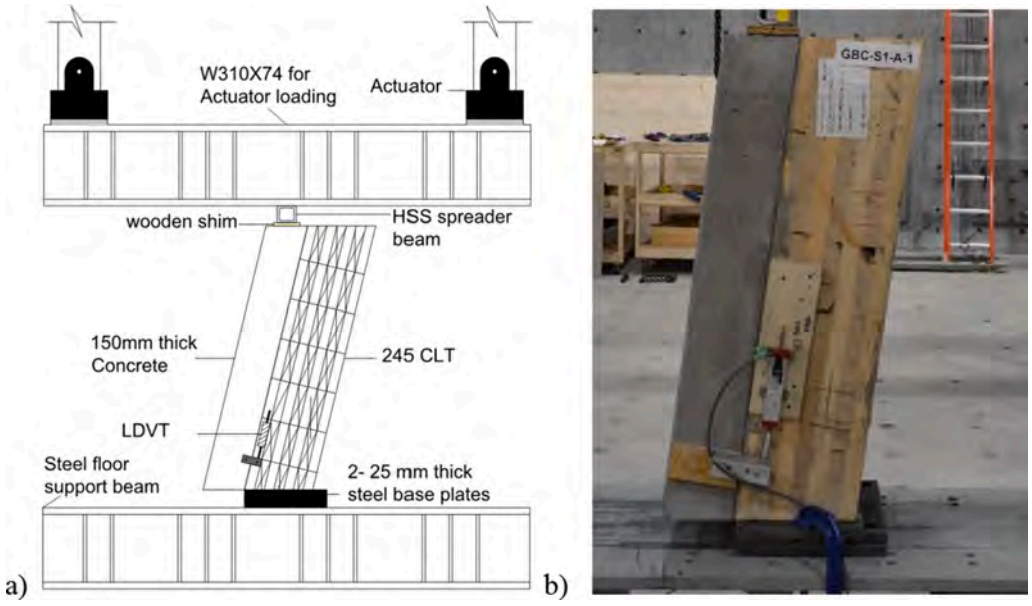

Fig. 3. (a) Schematic of small-scale test setup, and (b) photo of a test setup.

$$EI_{app} = \frac{\Delta F}{48\Delta d}\left(3L^2a - 4a^3\right) \quad (3)$$

where, ΔF is the change in forces between 10 and 40% of F_{max}, Δd is the corresponding change in deflection, L is the span, and a is the distance between the support and loading points.

3. Results and discussion

3.1. Small scale shear tests

The load–deflection curves from the individual small-scale steel kerf plate connector tests are illustrated in Fig. 6a, b, and c, whereas the

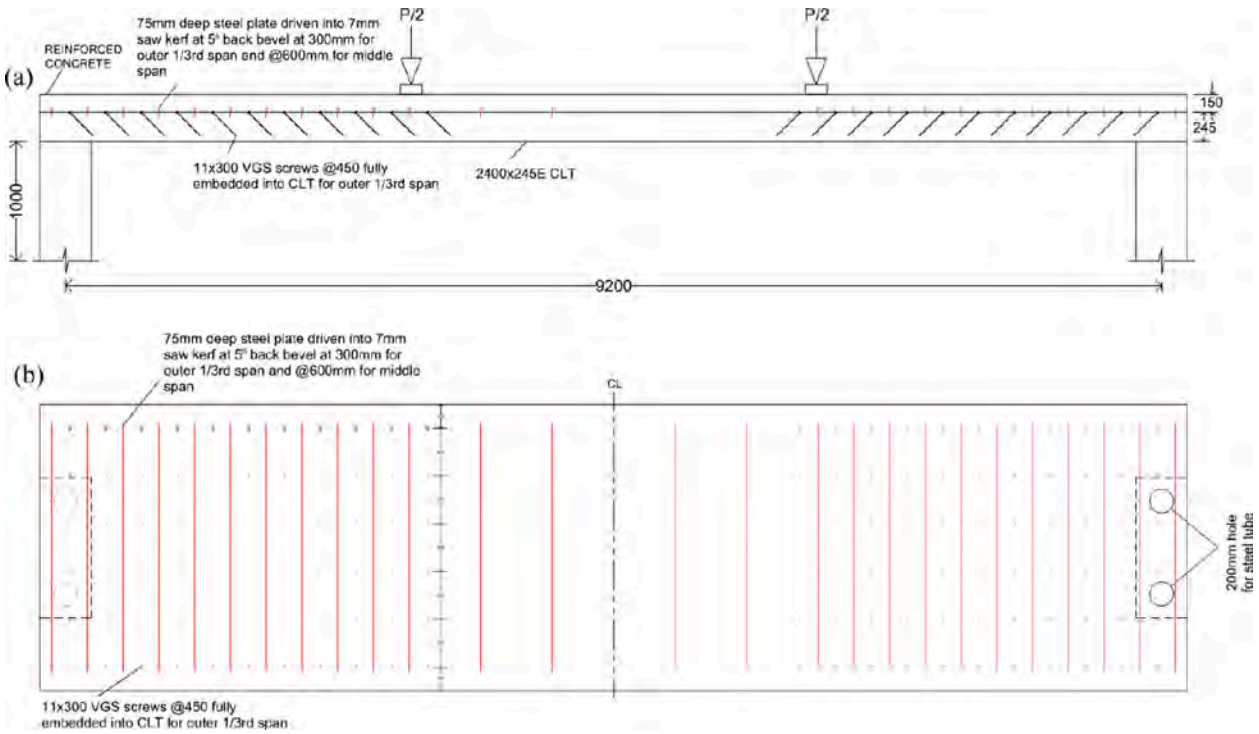

Fig. 4. Full-scale TCC floor specimens - a) cross-section, b) plan.

average load-deformations are plotted in Fig. 6d. The connections exhibited an elastic (almost linear) phase, a yield phase and failure; the six replicates from each group performed very consistently. Independent of the steel-plate embedment depth, yielding started at a deformation of just below 1 mm, indicating that yielding was only related to the steel-plates and no crushing deformation in the CLT panel occurred during the elastic phase. However, the connectors' post-yield behaviours were different between the various embedment depths. Connector Type A with 35 mm embedment did not exhibit any increase in load-carrying capacity beyond the yield point but did provide the largest deformation capacity with very little loss in loads until reaching deformation of approximately 10 mm. In contrast, connector Types B and C with 70 mm and 90 mm embedment, respectively, did exhibit load increases beyond the yield point. However, once ultimate load-carrying capacities were reached, these two connector types provided only small deformation capacities with a steep decrease in load after reaching its maximum. It can be postulated that these differences in deformation behaviour were caused by the different anchoring effects related to the different embedment depths. And it can be concluded that Connector Type A provided the most beneficial deformation behaviour.

The result metrics are summarized in Table 2. Type A connectors had the lowest load-carrying capacity, yield, and ultimate strengths (F_{max} = 350 kN; F_y = 332 kN; F_u = 280 kN). These metrics for Type B and Type C connectors were slightly higher, i.e. on average 7% and 5%, respectively. Variability between replicates within the test series was small with a coefficient of variations (CoV) around 4–7% for F_{max}, F_y and F_u.

All three connector types started yielding at similar deformations of between 0.8 and 0.9 mm. Type A connectors reached the largest deformations at maximum load and ultimate load (d_{Fmax} = 3.3 mm; d_u = 12.6 mm). The deformations of Type B and Type C connectors were significantly smaller (Type B: d_{Fmax} = 2.9 mm, d_u = 8.1 mm; Type C: d_{Fmax} = 3.0 mm, d_u = 6.0 mm), showing the reduction in deformation capacity when the kerf plates were embedded beyond the first layer of CLT. Variability of deformation was between 17% and 23%.

The stiffnesses observed both at serviceability and ultimate loads for Type A (K_{ser} = 416 kN/mm; K_u = 444 kN/mm), Type B connectors (K_{ser} = 395 kN/mm; K_u = 421 kN/mm), and Type C connectors (K_{ser} = 438 kN/mm; K_u = 453 kN/mm) were similar. The stiffness of Type A and Type C connectors were slightly higher when the kerf plates embedded into the stiffer (major axis) layers of the CLT panels (1st and 3rd layer, respectively).

The average ductility, calculated from the EEEP curves, for connector Type A was the highest with 15.4. Ductility decreased with the increase in kerf plate embedment depth. The values for Type B and Type C were 9.0 and 7.6, respectively, being 42% and 51%, respectively, lower compared to the ductility achieved by connector Type A.

Photos of failed specimens are provided in Fig. 7. Both Type A and Type C connectors caused concrete shear failure near the support. The shear cracks initiated when the specimens reached their ultimate loads. On the contrary, the failure in Type B connectors was due to the rolling shear failure of the CLT because the kerf plates were embedded into the weak cross-layer of the CLT panels.

3.2. Discussion of small scale shear tests

Based on the small-scale connector tests (cf. Table 2), increasing the embedment depth of the steel plates from 35 mm to 70 mm led to small increases of yield, maximum and ultimate load-carrying capacities. The stiffness (K_{ser}) of Type B (70 mm embedment) decreased by 5% compared to Type A due to the embedment into the transverse CLT layer. Importantly, anchoring the steel kerf plates in the minor strength axis layer was accompanied by a shift in the failure mode from concrete crushing to CLT rolling shear failure. This type of failure is not desirable and should be avoided; therefore, anchoring the steel kerf plates in the minor strength axis layer is not recommended.

Increasing the embedment depth from 35 mm to 90 mm did not improve the yield, maximum and ultimate load-carrying capacities. On the contrary, this increase in plate embedment depth decreased the deformation capacity and ductility of the connection. The embedment of the steel plates into the third layer did not offer a significant increase in stiffness; K_{ser} increased by 5% after increasing the embedment by 157% when compared to Type A. In summary, increasing the embedment depth beyond first layer of the CLT panel did not offer any improvement in the composite connection performance, therefore, the floor specimens

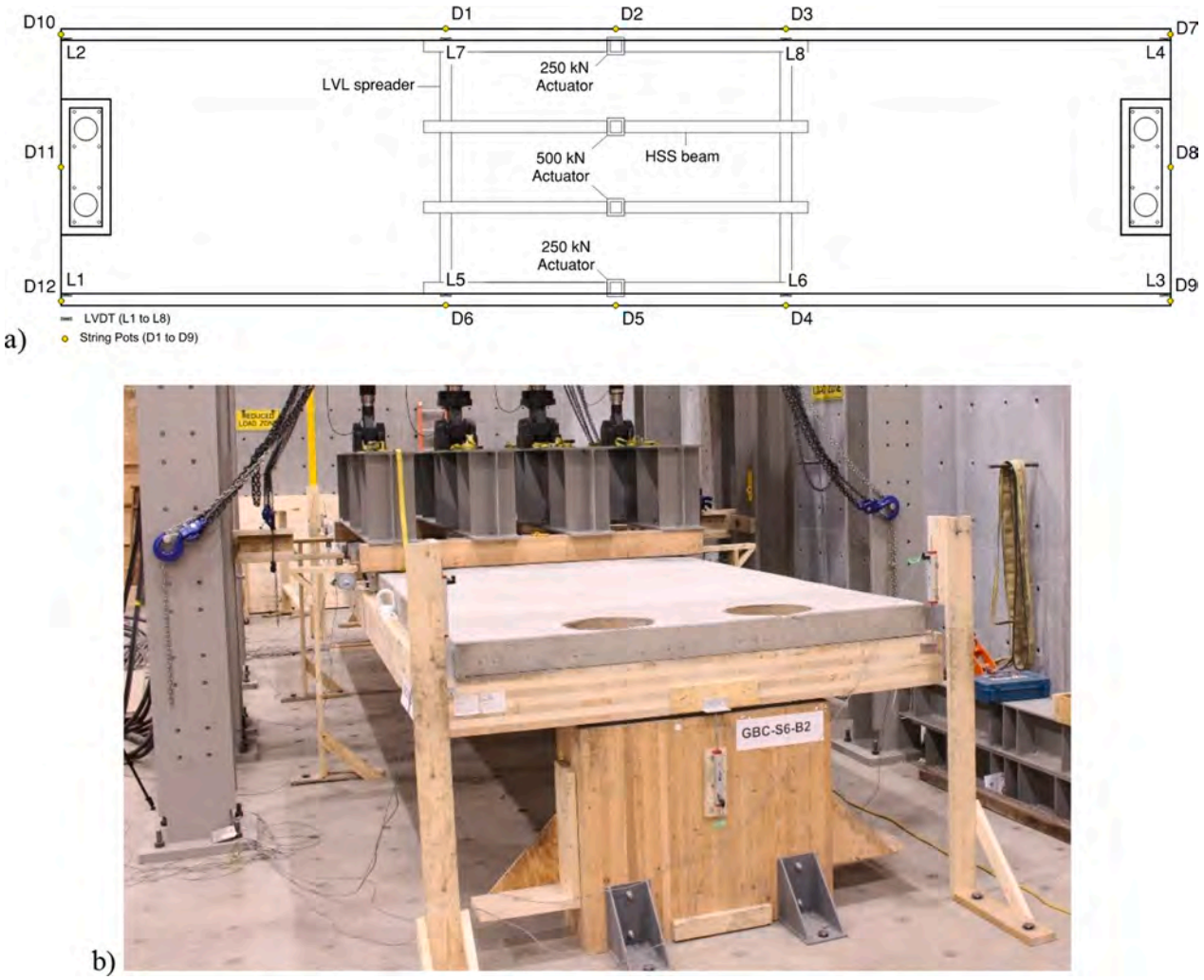

Fig. 5. Schematic (a) and photo (b) of a full-scale bending test setup.

for the full-scale testing were manufactured with Type A steel plate connectors.

The variation of K_{ser} observed in the small-scale tests was up to 23%, which is within the common range of stiffness variability of timber connections. While connection stiffness impact the overall effective bending stiffness and in results also the vibration performance of TCC floors, the potential impact of the observed variability in the small-scale connection stiffness on the floor vibration performance was outside the scope of this study.

3.3. Full-scale bending tests

The mid-span load–deflection curves of the full-scale TCC specimens are illustrated in Fig. 8. The load–displacement behaviours of both floor panels were approximately the same until failure. The load–displacement behaviours of both floor panels were approximately the same until failure. Similar, to the small-scale connections tests, the floors exhibited an elastic (almost linear) phase, a yield phase and failure, indicating that the floor performance can be traced back to the connector properties, of course in addition to the material properties. The pre-loading cycles that reducing the load from 40% to 10% of estimated capacity led to only a negligible increase in stiffness, demonstrating that there was almost no initial alignment behaviour of the floor system. Failure was accompanied by multiple small decreases in the load with increasing deformation, indication that a load-distribution occurred from damaged wood lamellas to undamaged ones.

The panels failed in bending at an average load of 1,040 kN (creating a maximum moment at the failure of 1,619 kNm) and a displacement at the failure of on average 124 mm, cf. Table 3.

The full-scale TCC floors' flexural capacity and demands are plotted in Fig. 9. The demands were estimated at ultimate and serviceability limit states with a live load of 4.8 kPa and 2.4 kPa. The short-term load duration factor, $K_D = 1.15$ was applied when estimating the demands of the specimens. With a live load of 2.4 kPa, the design flexural demands on the slab bands at ultimate and serviceability limit states were estimated as 756 kNm and 566 kNm, respectively. At service and ultimate loads, the average capacity/demand ratio for the half-reinforced full-scale TCC specimens was 2.9, and 2.2, respectively. At service loads, the average mid-span deflection observed in the full-scale TCC specimens was 42 mm.

Fig. 10 shows the CLT-concrete interface slips measured at 8 different locations along the length of the TCC floors. The parameters $d_{sl,0}$, $d_{sl,1/3L}$, $d_{sl,2/3L}$, $d_{sl,L}$ shows the average slips measured on both sides of the TCC floors at both panel ends ($d_{sl,0}$, $d_{sl,L}$) and the panel third points ($d_{sl,1/3L}$, $d_{sl,2/3L}$). In general, slips were very small and reached maximum values of approximately 0.4 mm at failure, clearly demonstrating the very high composite action achieved by the kerf plate connectors. The average slips near the supports were higher compared to third points; however, there was a small difference between the two test specimens. While for specimen HR-1, the end slips were almost twice those observed for one third point (L1 and L5) and approximately 25% larger that the slips observed for the other third point (L3 and L6), in specimen HR-2,

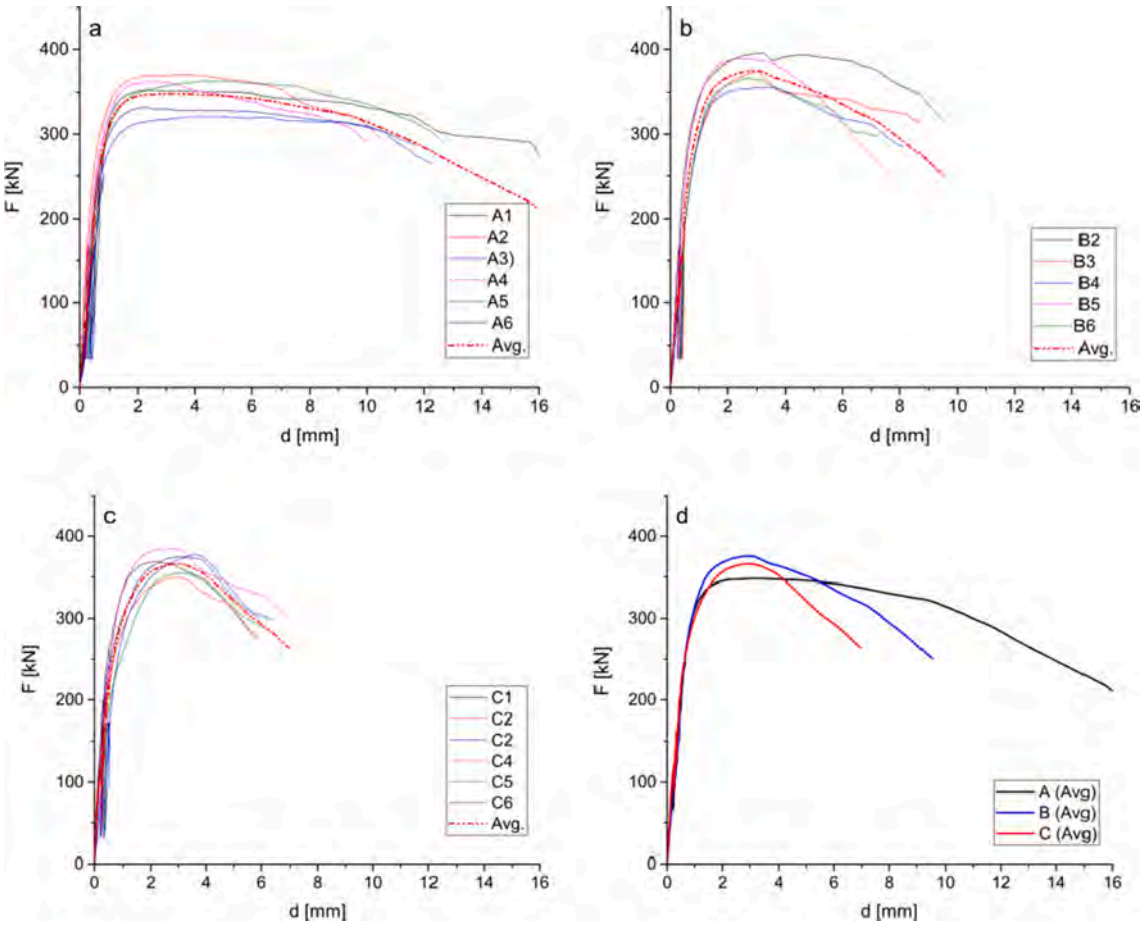

Fig. 6. Small-scale test load–deflection curves: a) S1-A; b) S1-B; c) S1-C; d) average curves.

Table 2
Small-scale tests for series S1.

ID	F_{max} [kN]	d_{Fmax} [mm]	K_{ser} [kN/mm]	K_u [kN/mm]	F_y [kN]	d_y [mm]	F_u [kN]	d_u [mm]	D [–]
A-1	352	2.4	340.5	356.7	342	1.0	282	13.3	13.2
A-2	371	3.7	583.5	574.6	350	0.6	297	10.3	17.2
A-3	321	4.1	333.7	416.6	306	0.9	256	13.4	14.7
A-4	362	2.6	465.3	475.4	338	0.7	290	10.0	13.8
A-5	363	4.9	410.1	432.6	346	0.8	291	12.4	14.7
A-6	332	2.3	361.2	410.4	308	0.9	266	16.1	18.9
Mean	**350**	**3.3**	**416**	**444**	**332**	**0.8**	**280**	**12.6**	**15.4**
CoV	6%	31%	23%	17%	6%	17%	6%	18%	14%
B-1	Specimen failed prematurely at support								
B-2	395	3.2	521	541	375	0.7	316	9.4	13.0
B-3	375	3.0	327	357	339	1.0	300	10.2	9.8
B-4	356	3.3	335	364	332	1.0	285	8.1	8.2
B-5	389	2.3	457	479	382	0.8	311	5.3	6.3
B-6	367	2.8	338	363	339	1.0	294	7.5	7.4
Mean	**376**	**2.9**	**395**	**421**	**354**	**0.9**	**301**	**8.1**	**9.0**
CoV	4%	13%	22%	20%	7%	15%	4%	24%	29%
C-1	369	2.2	511	573	353	0.7	295	5.0	7.3
C-2	349	3.0	455	474	325	0.7	280	5.8	8.1
C-3	377	3.6	314	331	349	1.1	302	5.9	5.3
C-4	384	2.7	477	476	356	0.7	308	6.5	8.7
C-5	355	3.2	346	346	325	0.9	284	6.3	6.7
C-6	374	3.1	523	521	342	0.7	299	6.3	9.7
Mean	**368.1**	**3.0**	**438**	**453**	**342**	**0.8**	**294**	**6.0**	**7.6**
CoV	4%	17%	20%	21%	4%	22%	4%	9%	20%

the end point slips were consistently 25% larger than the third point slips at failure. These small differences can safely be deemed inconsequential to the floor performance as shown in the overall floor performance.

The initial failure in the full-scale TCC specimens happened in the connector with the final subsequent failure occurred at mid span due to

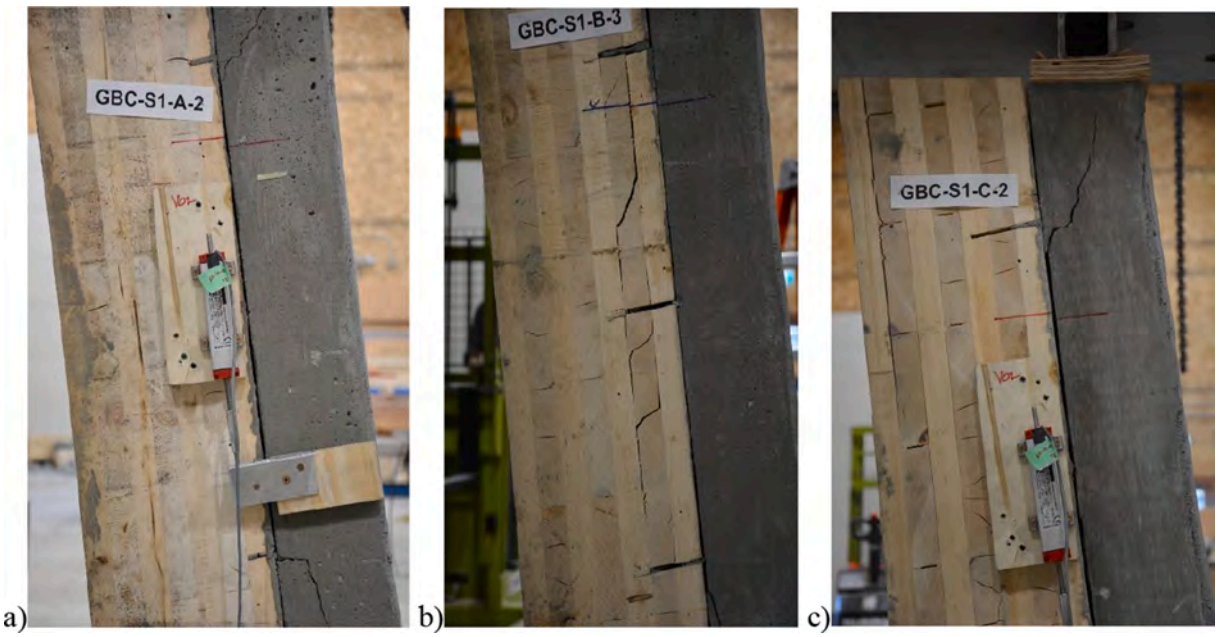

Fig. 7. Failure in small-scale tests: a) S1-A, b) S1-B, and c) S1-C.

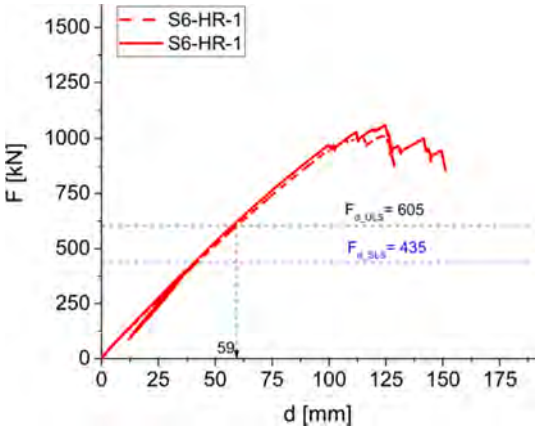

Fig. 8. Load-deflection curves of full-scale specimens.

Table 3
Full-scale test results.

ID	F_{max} [kN]	$M_{capcity}$ [kN.m]	$V_{capcity}$ [kN]	d_{Fmax} [mm]	k_s [kN/mm]	Failure [-]
S6-HR-1	1018	1586	509	123	25	Bending
S6-HR-2	1061	1653	531	125	26	Bending

ID	d_c	d_l	d_r	$d_{sl,0}$	$d_{sl,1/3L}$	$d_{sl,2/3L}$	$d_{sl,L}$
	[mm]	[mm]	[mm]	[mm]	[mm]	[mm]	[mm]
S6-HR-1	123	113	107	0.5	0.3	0.3	0.4
S6-HR-2	125	110	110	0.4	0.4	0.5	0.5

bending, see Fig. 11a. The warping, i.e., upward weak axis deflection at the support, is shown in Fig. 11b.

3.4. Comparison to expected composite performance

The performance of the TCC floors was estimated based on the γ-method using the stiffness values recorded from the small-scale tests, cf. Table 2. The γ values for ultimate (γ_u) and serviceability (γ_{ser}) limit states for the floors with kerf plates are presented in Table 4. In this context, it should be reminded that the gamma method requires the connectors to be spaced along the length of the floor span so that the maximum distance does not exceed four times the minimum distance. The full-scale floors tested herein met this requirement. Based on these, the expected effective composite stiffness, EI_{cal} and the expected load-carrying capacity, F_{cal}, were computed and compared against the experimentally obtained load-carrying capacity, F_{max}, and the apparent bending stiffness, EI_{app}, respectively. The experimental capacity observed F_{max} exceeds calculated capacity F_{cal} by 60% to 70% since 5th percentile specified strength values (cf. Table 2) were used. The ratio EI_{app}/EI_{cal_u} is close to 1.0 demonstrating the adequacy of applying the gamma method to predict the performance of TCC composite floors.

4. Discussion

The TCC connector's properties e.g., load-carrying capacity, stiffness, and ductility were determined based on small-scale tests. Except for the specimen size, all CLT and concrete material properties, connector size, embedment depth and spacing, and concrete reinforcement were the same in the full-scale specimens. The stiffness properties obtained from the small-scale tests were utilized in the γ-method to predict the performance of the full-scale TCC specimens under four-point bending.

The gamma method as presented in Eurocode 5 [14] allowed estimating the composite action and the effective bending stiffness of TCC floors, as well as computing the stresses in timber, concrete and shear connector part of the timber-concrete composite section. While outside the scope of the presented research, future work could investigate the feasibility of an analytical model with respect to the impact of the kerf plate embedment depth regarding the failure mechanism in the CLT as well as the effectiveness of different reinforcements to increase the shear

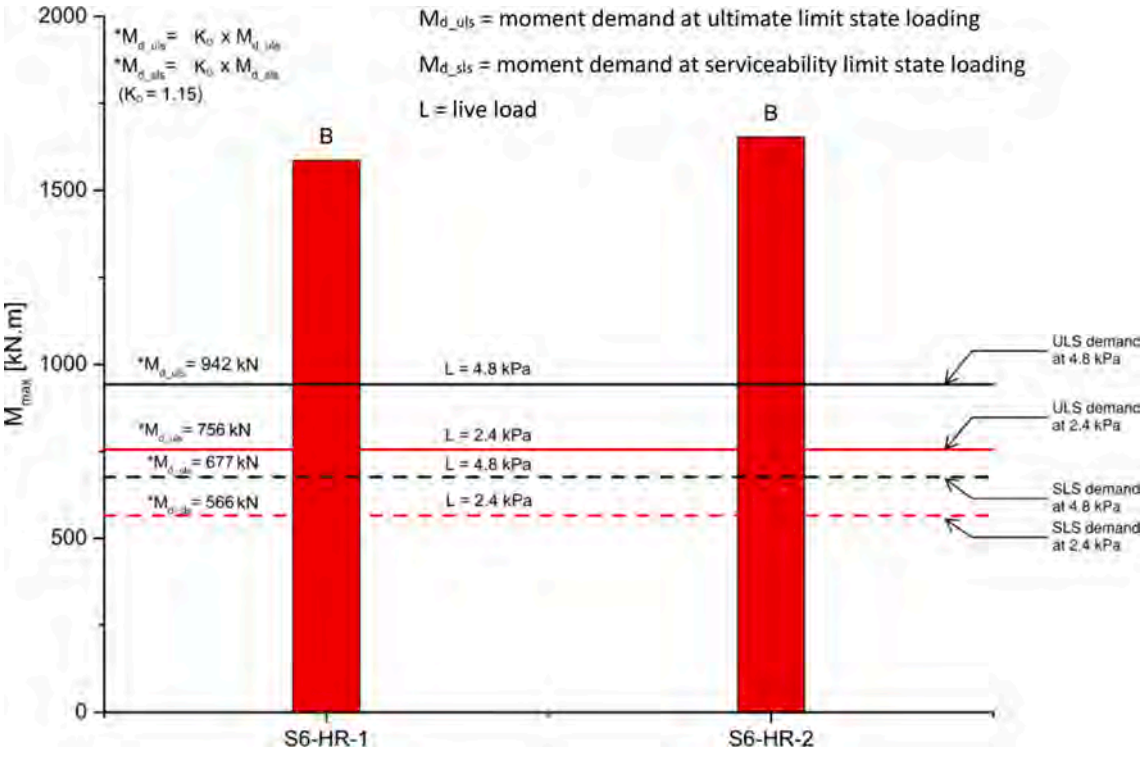

Fig. 9. Capacity vs demand comparison for full-scale specimens.

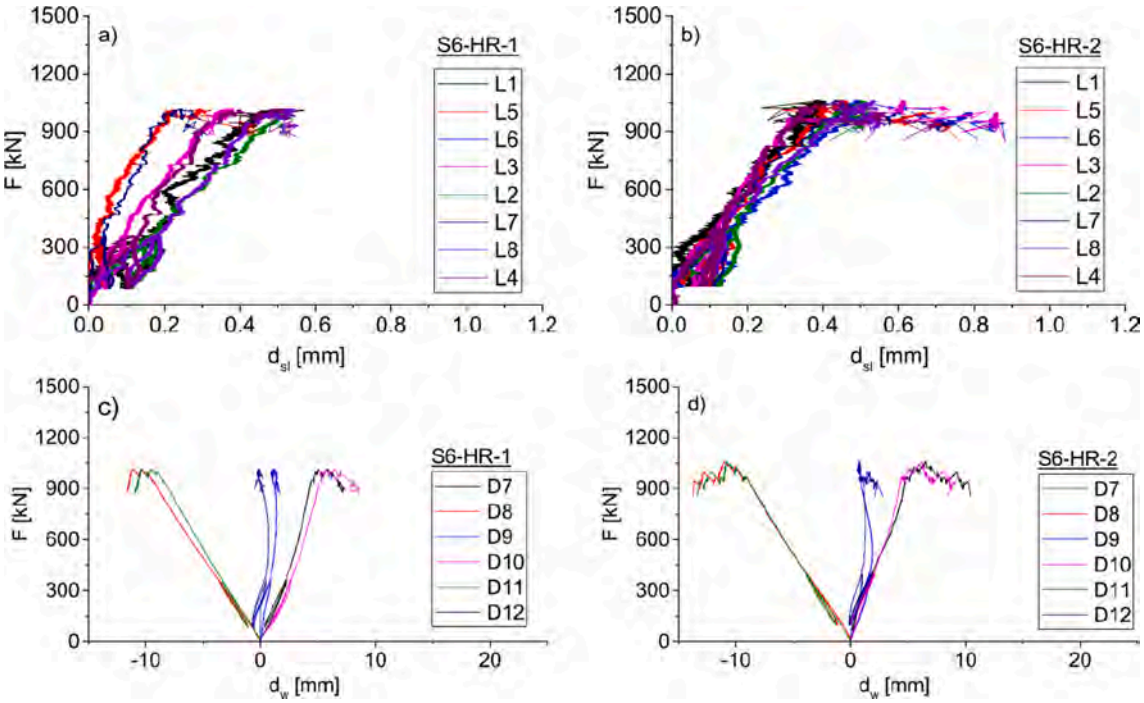

Fig. 10. Slips at CLT-concrete interface (a,b) and warping at supports (c,d).

resistance of CLT panels in regions of high stresses where the steel kerf plates are installed.

In addition to the excellent mechanical performance, the steel kerf plate connectors were easy to install and, as an off-the-shelf product, are available at a significantly lower cost than other shear connectors for TCC systems such as STS and HBV perforated plates. The kerf plates can be pre-installed into TCC floor specimens which leads to a reduction in construction time. In addition, the kerf plates facilitate the placement of the concrete rebar cages which improves the on-site constructability.

5. Conclusions

This research evaluated the performance of TCC floor systems floors with steel kerf plates as shear connectors. The following key conclusions

Fig. 11. (a) Typical bending failure in full-scale TCC floors; (b) warping (upward deflection) at support.

Table 4
Comparison of test results versus predictions.

ID	γ_{ser}	γ_u	EI_{app}	EI_{cal}	F_{cal}	F_{max}/F_{cal}	EI_{app}/EI_{cal}
	[–]	[–]	[kNm^2]	[kNm^2]	[kN]	[–]	[–]
S6-HR-1	0.95	0.92	130,987	141,600	625	1.63	0.93
S6-HR-2	0.95	0.92	134,879	141,600	625	1.70	0.95

can be drawn:

- Small-scale shear tests demonstrated that the kerf plates provided a very stiff and strong connector option for TCC floor systems.
- Specimens with the steel plate edges embedded in the longitudinal CLT layer failed in concrete shear, while embedment in the transverse layer led to rolling shear failure in the cross layer.
- Embedding the kerf plates into the top layer of the CLT panels (herein 35 mm) provided the best connector performance with the highest deformation capacity and ductility. Increasing the kerf plate embedment depth decreased the deformation capacity and ductility.
- Using steel kerf plates as shear connector allows designing TCC floors with high effective bending stiffness and very high composite efficiency, with gamma values close to 1.0.
- The bending stiffness of the TCC floors (*EI*) was predicted using the gamma method. The ratio between experimental and expected (close to 1.0) demonstrated the adequacy of applying the gamma method to predict the performance of TCC composite floors.

The results from this research were utilized to make project-specific design decisions for "The Arbour", a 10-storey mass timber building for George Brown College, located in Toronto, Canada.

CRediT authorship contribution statement

Md Shahnewaz: Conceptualization, Methodology, Investigation, Formal analysis, Visualization, Writing – original draft. **Robert Jackson:** Conceptualization, Methodology, Investigation, Supervision. **Thomas Tannert:** Conceptualization, Methodology, Investigation, Supervision, Writing – review & editing.

Declaration of Competing Interest

The authors declare that they have no known competing financial interests or personal relationships that could have appeared to influence the work reported in this paper.

Acknowledgements

Natural Resources Canada, through the Green Construction through Wood (GCWood) program [40], assisted with the project costs including a test program to support the innovative use of long-span TCC floors. The support by the UNBC technicians Michael Billups and Ryan Stern and undergraduate research assistant Anthony Bilodeau are greatly appreciated.

References

[1] M. Green, E. Karsh. The case for tall wood buildings, Wood Enterprise Coalition, 2012, Vancouver, BC, Canada.
[2] T. Tannert, M. Follesa, M. Fragiacomo, P. Gonzalez, H. Isoda, D. Moroder, Seismic design of cross-laminated timber buildings, Wood Fiber Sci. 50 (2018) 3–26.
[3] R. Brandner, G. Flatscher, A. Ringhofer, G. Schickhofer, A. Thiel, Cross laminated timber (CLT): overview and development, Eur. J. Wood Wood Prod. 74 (3) (2016) 331–351.
[4] S. Gagnon, C. Pirvu, Cross Laminated Timber (CLT) Handbook, FPInnovations, 2020, Vancouver, BC, Canada.
[5] D. Yeoh, M. Fragiacomo, M. De Franceschi, K. Heng Boon, State of the art on timber-concrete composite structures: Literature review, J. Struct. Eng. 137 (10) (2011) 1085–1095.
[6] A.M.P.G. Dias, J. Skinner, K. Crews, T. Tannert, Timber-concrete-composites increasing the use of timber in construction, Eur. J. Wood Wood Prod. 74 (3) (2016) 443–451.
[7] M. Li, Evaluating rolling shear strength properties of cross-laminated timber by short-span bending tests and modified planar shear tests, J. Wood Sci. 63 (4) (2017) 331–337.
[8] T. Ehrhart, R. Brandner, Rolling shear: Test configurations and properties of some European soft-and hardwood species, Eng. Struct. 172 (2018) 554–572.
[9] CSA O86-19, Engineering Design in Wood, Canadian Standard Association, 2019, Ottawa, ON, Canada.
[10] P. Dietsch, R. Brandner, Self-tapping screws and threaded rods as reinforcement for structural timber elements–a state-of-the-art report, Constr. Build. Mater. 97 (2015) 78–89.
[11] T. Tannert, F. Lam, Self-tapping screws as reinforcement for rounded dovetail connections, Struct. Control Health Monit. 16 (3) (2009) 374–384.
[12] Mass Timber Institute. John H. Daniels Faculty of Architecture, University of Toronto. https://academic.daniels.utoronto.ca/masstimberinstitute/ [Accessed April 2021].
[13] J. Weckendorf, T. Toratti, I. Smith, T. Tannert, Vibration serviceability performance of timber floors, Eur. J. Wood Wood Prod. 74 (3) (2016) 353–367.
[14] CEN EN 1995: Eurocode 5, design of timber structures, European Committee for Standardization, 2004, Brussels, Belgium.
[15] Möhler K. Über das Tragverhalten von Biegeträgern und Druckstäben mit zusammengesetzten Querschnitten und nachgiebigen Verbindungsmitteln, 1956, Doctoral dissertation, Karlsruhe, Germany.
[16] A.M.P.G. Dias, S.M.R. Lopes, J.W. Van de Kuilen, H.M.P. Cruz, Load-carrying capacity of timber concrete joints with dowel-type fasteners, J. Struct. Eng. 133 (5) (2007) 720–727.
[17] A.M.P.G. Dias, U. Kuhlmann, K. Kudla, S. Mönch, Performance of dowel-type fasteners and notches for hybrid timber structures, Eng. Struct. 171 (2018) 40–46.
[18] H. Du, X. Hu, Z. Xie, H. Wang, Study on shear behavior of inclined cross lag screws for glulam-concrete composite beams, Constr. Build. Mater. 224 (2019) 132–143.
[19] M. Derikvand, G. Fink, Deconstructable connector for TCC floors using self-tapping screws, J. Build. Eng. 42 (2021), 102495.
[20] L. Marchi, R. Scotta, L. Pozza, Experimental and theoretical evaluation of TCC connections with inclined self-tapping screws, Mater. Struct. 50 (3) (2017) 1–15.
[21] P. Clouston, A. Schreyer, Design and use of wood-concrete composites, Practice Period. Struct. Des. Constr. 13 (4) (2008) 167–174.
[22] S.C. Auclair, L. Sorelli, A. Salenikovich, A new composite connector for timber concrete composite structures, Constr. Build. Mater. 112 (2016) 84–92.
[23] T. Tannert, B. Endacott, M. Brunner, T. Vallée, Long-term performance of adhesively bonded timber-concrete composite, Int. J. Adhes. Adhes. 72 (2017) 51–61.
[24] T. Tannert, A. Gerber, T. Vallee, Hybrid adhesively bonded timber-concrete-composite floors, Int. J. Adhes. Adhes. 97 (2019), 102490.
[25] W. Zhu, H. Yang, W. Liu, B. Shi, Z. Ling, H. Tao, Experimental investigation on innovative connections for timber–concrete composite systems, Constr. Build. Mater. 207 (2019) 345–356.
[26] B. Shi, W. Liu, H. Yang, Experimental investigation on the long-term behaviour of prefabricated timber-concrete composite beams with steel plate connections, Constr. Build. Mater. 266 (2021), 120892.
[27] D. Yeoh, M. Fragiacomo, M. De Franceschi, A.H. Buchanan, Experimental Tests of Notched and Plate Connectors for LVL-Concrete Composite Beams, J. Struct. Eng. (2011), https://doi.org/10.1061/ASCEST.1943-541X.0000288.
[28] L. Zhang, Y.H. Chui, D. Tomlinson, Experimental investigation on the shear properties of notched connections in mass timber panel-concrete composite floors, Constr. Build. Mater. 234 (2020), 117375.
[29] Y. Jiang, R. Crocetti, CLT-concrete composite floors with notched shear connectors, Constr. Build. Mater. 195 (2019) 127–139.
[30] A. Siddika, M.A. Al Mamun, F. Aslani, Y. Zhuge, R. Alyousef, A. Hajimohammadi, Cross-laminated timber–concrete composite structural floor system: a state-of-the-art review, Eng. Fail. Anal. 130 (2021), 105766.
[31] S. Lehmann, M. Grosse, K. Rautenstrauch, New connector types of laminated timber-concrete composite element joints, in: Proceedings of the International RILEM Symposium, 2001, pp. 301–310.
[32] Aspect Structural Engineers, Microsoft Silicon Valley Campus, http://aspectengineers.com/portfolio/microsoft-silicon-valley/ [Accessed April 2021].
[33] ANSI/APA PRG 320, Standard for Performance-Rated Cross-Laminated Timber. American National Standards Institute, 2017, New York, USA.
[34] ASTM C39. Standard test method for compressive strength of cylindrical concrete specimens, American Society for Testing and Materials, West Conshohocken, USA, 2021.
[35] ASTM A36. Standard Specification for Carbon Structural Steel, American Society for Testing and Materials, West Conshohocken, USA, 2019.
[36] ETA-11/0030, Rothoblaas Self-tapping screws and threaded rods. Screws and threaded rods for use in timber constructions, 2020.
[37] EN 408, Timber structures—Structural timber and glued laminated timber—Determination of some physical and mechanical properties, European Committee for Standardization (CEN), 2010, Brussels, Belgium.
[38] EN 26891, Timber structures—Joints made with mechanical fasteners—General principles for the determination of strength and deformation characteristics, European Committee for Standardization (CEN), 2013, Brussels, Belgium.
[39] Astm E2126, Standard test methods for cyclic (reversed) load test for shear resistance of walls for buildings 2011 West Conshohocken, USA.
[40] Natural Resources Canada (NRCAN), Green Construction through Wood (GCWood) Program, https://www.nrcan.gc.ca [Accessed September 2020].